

Received February 22, 2020, accepted February 29, 2020, date of publication March 6, 2020, date of current version March 19, 2020.

Digital Object Identifier 10.1109/ACCESS.2020.2978025

A Comparative Study of the Joint Neuro-Fuzzy Friction Models for a Triple Link Rotary Inverted Pendulum

ZIED BEN HAZEM, MOHAMMAD JAVAD FOTUHI, (Student Member, IEEE),
AND ZAFER BINGÜL , (Member, IEEE)

Automation Research Laboratory, Mechatronics Engineering Department, Kocaeli University, 41001 Kocaeli, Turkey

Corresponding author: Zafer Bingül (zaferb@kocaeli.edu.tr)


This work was supported by partial finance from the Scientific Research Projects Coordination Unit of Kocaeli University.

ABSTRACT In this paper, Neuro-Fuzzy Friction Estimation Models (NFFEM) are developed to estimate the joint friction coefficients in a Triple Link Rotary Inverted Pendulum (TLRIP) system and compared with an Adaptive Friction Estimation Models (AFEM). The different versions of AFEMs and NFFEMs are generated based on each of the following friction estimation models: Non-Conservative Friction Model (NCFM), Linear Friction Model (LFM), and Non-Linear Friction Model (NLFM). The aim of this study is to obtain joint friction models which depend on both velocity and acceleration in a large range of motion trajectory that involves difficult and sudden large changes. In the proposed NFFEMs, joint velocities and accelerations of the TLRIP are used as the input variables of the Neuro-Fuzzy system trained by using a Radial Basis Function Artificial Neural Network (RBANN). Several experiments are conducted on TLRIP system to verify the NFFEMs. In order to determine the estimation performance of the friction models, total Root Mean Squared Errors (RMSE) between position simulation results obtained from each joint friction model and encoders in the experimental setup are computed. Based on the position RMSEs, the NFFEMs produces much better estimation results than the AFEMs. Among NFFEMs, the neuro-fuzzy nonlinear friction model (NFNLM) gives the best results.

INDEX TERMS Triple link rotary inverted pendulum (TLRIP), neuro-fuzzy friction estimation and modelling.

I. INTRODUCTION

A rotary Inverted Pendulum System (RIPS) is one of the most interesting and popular mechatronic systems that can exist in many different forms [2]. It is a challenging problem in the area of control engineering applications in linear and nonlinear control, also can be called “Furuta Pendulum” [3]. Furuta Pendulum is a simple structure that consists of a high torque servo motor which rotates in the horizontal plane where the pendulums are attached to the horizontal arm which is free to rotate in the vertical plane [4]. The Furuta pendulum system was developed by K. Furuta at Tokyo Institute of Technology and was called the “TITECH pendulum” [5]. Due to the gravitational forces and the coupling arising from the Coriolis and centripetal forces, the system is underactuated, unstable and extremely nonlinear [6]. The RIPS include a nonlinearity

The associate editor coordinating the review of this manuscript and approving it for publication was Hamid Mohammad-Sedighi .

due to the frictions in the joints. RIPS is the most convenient example to understand the influence of the joint frictions on the design and performance of feedback controllers that aim to stabilize the pendulum in the upright position. The frictions can have high nonlinear values which result in steady-state errors, limit cycles, and poor performance of the system [7]. It has an influence on the system’s response that should be considered seriously [8]. Therefore, friction estimation has the potential to ameliorate the quality and dynamic behavior of the system [9].

In [1], the AFEMs were developed to estimate the friction coefficients for TLRIP system. In this AFEM approach, the joint accelerations of the TLRIP were classified into three groups: low, medium and high. The adaptive friction coefficients were optimized according to this acceleration classification. In this paper, the NFFEMs were developed using Neuro-Fuzzy (NF) system. The joint velocities and accelerations of the TLRIP as the input variables were applied

to NF. Membership functions of input and output variables and fuzzy rules in the fuzzy estimation system were trained using a Radial Basis Function Artificial Neural Network (RBANN). The variable friction coefficients of NFFEMs were estimated and verified through several simulation and experimental results. These proposed friction estimation models are compared with AFEMs in [1]. This work has three important contributions to the literature. Firstly, all friction models in the literature depend only on velocity, however, the friction model developed here depends on both velocity and acceleration. This approach has enabled us to obtain a two-dimensional friction model. Secondly, the coefficients of all friction models in the literature were constant when the physical quantities changes. On the other hand, the coefficients of the friction models in this work vary depending on the state of the velocity and acceleration. Hence, this friction model allows for better estimation of the effects of friction in different velocity and acceleration conditions. Thirdly, much of existing papers in the literature have studied only the frictions of the linear motion which depends on linear velocity and force. This paper examines frictions on the joints which have hard rotational motions. This paper is organized as follows: An analytical model and a numerical mathematical model based on Matlab/SimMechanics of the TLRIP are presented in section II. Section III presents the frictions' estimation models. In Section IV, the Neuro-Fuzzy friction estimation model is presented. The experimental results have verified the effectiveness of the proposed approach in Section V. Finally, Section VI summarizes the conclusion of the work.

II. MATHEMATICAL MODELS AND SIMULATION

In this section, an analytic mathematical model and numeric simulation model (SimMechanics) of the TLRIP is explained in detail. The TLRIP is composed of a horizontal arm which is controlled by a torque servo motor, attached to three vertical arms [10]. A balance mass mounted on the horizontal arm to maintain the balance inertia of the system. The angle of the horizontal arm (θ_1) and the angles of three vertical arms (θ_2, θ_3 and θ_4) in TLRIP are illustrated in Figure 1. The three rotary pendulums have two equilibrium points in upright and downward positions. The motion equations of the TLRIP system are obtained by Newton-Euler equations [11]. The kinematic parameters and coordinate systems of the TLRIP based on the Denavit-Hartenberg (DH) convention method are shown in Figure 1. Model parameters and variables are given in Table 1. The physical parameters and DH parameters of the TLRIP are given in Table 2 and Table 3, respectively.

The dynamic torque equations of the TLRIP can be written in a matrix form, as follows:

$$M(\theta)\ddot{\theta} + C(\theta, \dot{\theta}) + \tau_f(\theta, \dot{\theta}) + G(\theta) = \tau_1 \quad (1)$$

where $\theta, \dot{\theta}$ and $\ddot{\theta}$ are the vectors of joint angles, the angular velocities and the angular accelerations respectively. $M(\theta)$ is the mass matrix, $C(\theta, \dot{\theta})$ is the Coriolis and Centripetal force vector, $\tau_f(\theta, \dot{\theta})$ is the friction torque vector, $G(\theta)$ is the

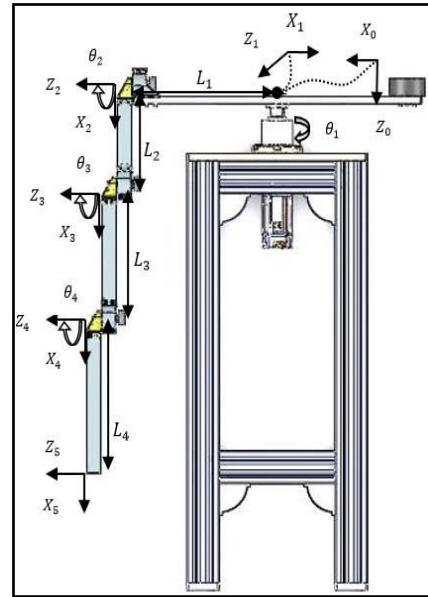


FIGURE 1. Kinematics parameters of the TLRIP.

TABLE 1. Model parameters and physical variables of the TLRIP.

Symbols	Explanation	Unit
θ_i	The angle of the i-th link	[rad]
τ_i	Torque for i-th link	[Nm]
I^i	Inertia tensor of i-th link	[kg · m ²]
I_{zzi}^i	Z-component of the inertia tensor of i-th link	[kg · m ²]
m_i	Mass of i-th link	[kg]
m_B	Mass of balance mass	[kg]
L_i	Length of i-th link	[m]
P_{Ci}^i	The mass centre position of an i-th link	[m]
g	Gravity	[N · kg ⁻¹]

TABLE 2. Mass and inertia parameters of the TLRIP.

m_1	3.1129	L_1	0.42021
m_2	0.7298	L_2	0.2675
m_3	0.6789	L_3	0.3650
m_4	0.45	L_4	0.4240
m_B	3.1469	G	9.81
I_{zz1}^1	0.25	I_{zz2}^2	0.04
I_{zz3}^3	0.05	I_{zz4}^4	0.05

TABLE 3. D-H parameters of the TLRIP.

Coordinate	α_{i-1}	A_{i-1}	d_i	θ_i
1	$\frac{\pi}{2}$	0	0	$\theta_1 + \frac{\pi}{2}$
2	$\frac{\pi}{2}$	0	L_1	θ_2
3	0	L_2	0	θ_3
4	0	L_3	0	θ_4
5	0	L_4	0	0

gravity vector and τ_1 is the command torque vector [12]. The matrix expression in the dynamic equation (1), the following

parameters are employed:

$$\begin{aligned}
 h_1 &= L_1^2 m_1, & h_2 &= L_1^2 m_2, & h_3 &= L_1^2 m_3, & h_4 &= L_1^2 m_4 \\
 h_5 &= L_2^2 m_2, & h_6 &= L_2^2 m_3, & h_7 &= L_2^2 m_4, & h_8 &= L_3^2 m_3 \\
 h_9 &= L_3^2 m_4, & h_{10} &= L_4^2 m_4, & h_{11} &= L_1 L_4 m_4, & h_{12} &= L_1 L_3 m_4 \\
 h_{13} &= L_1 L_3 m_3, & h_{14} &= L_2 L_3 m_3, & h_{15} &= L_2 L_4 m_4 \\
 h_{17} &= L_3 L_4 m_3, & h_{18} &= m_2 + 2m_3 + 2m_4, & h_{19} &= m_3 + 2m_4 \\
 h_{20} &= L_1 L_3, & h_{21} &= L_1 L_2, & h_{22} &= L_2 L_3, & h_{23} &= L_3 g m_3 \\
 h_{24} &= L_3 g m_4, & h_{25} &= L_4 g m_4, & h_{26} &= L_2 g, & h_{27} &= L_3 g \quad (2)
 \end{aligned}$$

The elements of the mass matrix become as follows:

$$\begin{aligned}
 M_{11} &= I_{zz1} + I_{zz2} + I_{zz3} + I_{zz4} + \frac{h_1}{4} + h_2 + h_3 + \frac{h_5}{8} + h_3 \\
 &+ \frac{h_{17} \cos \theta_4}{2} - \frac{h_{19} h_{22} \cos(2\theta_2 + \theta_3)}{2} + \frac{h_{15} \cos(\theta_3 + \theta_4)}{2} \\
 &- \frac{h_{15} \cos(2\theta_2 + \theta_3 + \theta_4)}{2} - \frac{h_{17} \cos(2\theta_2 + 2\theta_3 + \theta_4)}{2} \\
 &- \cos(2\theta_2 + 2\theta_3) \times \left(\frac{I_{zz3}}{2} + \frac{h_8}{8} + \frac{h_9}{2} \right) + \frac{h_6}{2} + \frac{h_7}{2} + \frac{h_8}{8} \\
 &- \cos(2\theta_2) \times \left(\frac{I_{zz2}}{2} + \frac{h_8}{8} + \frac{h_6}{2} + \frac{h_7}{2} \right) + \frac{h_{19} h_{22} \cos \theta_3}{2} \\
 &- \cos(2\theta_2 + 2\theta_3 + 2\theta_4) \times \left(\frac{h_{10}}{8} + \frac{I_{zz4}}{2} \right) + \frac{h_9}{2} + \frac{h_{10}}{8} \quad (3)
 \end{aligned}$$

$$\begin{aligned}
 M_{12} &= \frac{h_{18} h_{21} \cos(\theta_2)}{2} - \frac{h_{11} \cos(\theta_2 + \theta_3 + \theta_4)}{2} \\
 &- \frac{h_{19} h_{20} \cos(\theta_2 + \theta_3)}{2} \quad (4)
 \end{aligned}$$

$$\begin{aligned}
 M_{13} &= -\cos(\theta_2 + \theta_3) \times \left(\frac{h_{13}}{2} + h_{12} \right) \\
 &- \frac{h_{11} \cos(\theta_2 + \theta_3 + \theta_4)}{2} \quad (5)
 \end{aligned}$$

$$M_{14} = -\frac{h_{11} \cos(\theta_2 + \theta_3 + \theta_4)}{2} \quad (6)$$

$$\begin{aligned}
 M_{22} &= I_{zz2} + I_{zz3} + I_{zz4} + \frac{h_5}{4} + h_7 + \frac{h_8}{4} + h_9 + \frac{h_{10}}{4} \\
 &+ h_{17} \cos(\theta_4) + h_{17} \cos(\theta_4) + h_{15} \cos(\theta_3 + \theta_4) \\
 &+ \cos(\theta_3) \times (h_{14} + 2h_{16}) \quad (7)
 \end{aligned}$$

$$\begin{aligned}
 M_{23} &= I_{zz3} + I_{zz4} + \cos(\theta_3) \times \left(\frac{h_{14}}{2} + h_{16} \right) + \frac{h_8}{4} + h_9 \\
 &+ \frac{h_{10}}{4} + h_{17} \cos \theta_4 + \frac{h_{15} \cos(\theta_3 + \theta_4)}{2} \quad (8)
 \end{aligned}$$

$$M_{24} = I_{zz4} + \frac{h_{10}}{4} + \frac{h_{17} \cos \theta_4}{2} + \frac{h_{15} \cos(\theta_3 + \theta_4)}{2} \quad (9)$$

$$M_{33} = I_{zz3} + I_{zz4} + \frac{h_8}{4} + h_9 + \frac{h_{10}}{4} + h_{17} \cos \theta_4 \quad (10)$$

$$M_{34} = I_{zz4} + \frac{h_{10}}{4} + \frac{h_{15} \cos \theta_4}{2} \quad (11)$$

$$M_{44} = I_{zz4} + \frac{h_{10}}{4} \quad (12)$$

$$\begin{aligned}
 M_{31} &= M_{13}, & M_{32} &= M_{23}, & M_{41} &= M_{14} \\
 M_{42} &= M_{24}, & M_{43} &= M_{34} \quad (13)
 \end{aligned}$$

The mass 4 × 4 matrix is as follows below

$$M(\theta) = \begin{bmatrix} M_{11} & M_{12} & M_{13} & M_{14} \\ M_{21} & M_{22} & M_{23} & M_{24} \\ M_{31} & M_{32} & M_{33} & M_{34} \\ M_{41} & M_{42} & M_{43} & M_{44} \end{bmatrix} \quad (14)$$

The elements of Coriolis and centrifugal force are given as follows:

$$\begin{aligned}
 c_{11} &= \frac{1}{2} \left(h_{21} \dot{\theta}_2^2 \sin \theta_2 \times h_{18} \right) - \frac{1}{2} \left(h_{22} \dot{\theta}_1 \dot{\theta}_3 \sin \theta_3 \times h_{19} \right) \\
 &+ \frac{1}{4} \times \left(\dot{\theta}_1 \sin(2\theta_2 + 2\theta_3) \times (\dot{\theta}_2 + \dot{\theta}_3) \times (4I_{zz3} + h_8 + 4h_9) \right) \\
 &+ \frac{1}{4} \times \left(\dot{\theta}_1 \sin(2\theta_2 + 2\theta_3 + 2\theta_4) \times (h_{10} + 4I_{zz4}) \right) \\
 &\times \left(\dot{\theta}_2 + \dot{\theta}_3 + \dot{\theta}_4 \right) \\
 &- \frac{1}{2} \left(h_{15} \dot{\theta}_1 \sin(\theta_3 + \theta_4) \times (\dot{\theta}_2 + \dot{\theta}_3) \right) - \frac{1}{2} \left(h_{15} \dot{\theta}_2 \dot{\theta}_4 \sin \theta_4 \right) \\
 &+ \frac{1}{2} \left(h_{17} \dot{\theta}_1 \sin(2\theta_3 + 2\theta_3 + \theta_4) \times (2\dot{\theta}_2 + 2\dot{\theta}_3 + \dot{\theta}_4) \right) \\
 &+ \frac{1}{2} \left(h_{15} \dot{\theta}_1 \sin(2\theta_3 + \theta_3 + \theta_4) \times (2\dot{\theta}_2 + 2\dot{\theta}_3 + \dot{\theta}_4) \right) \\
 &+ \frac{1}{4} \left(\dot{\theta}_1 \dot{\theta}_2 \sin(2\theta_2) \times (4I_{zz2} + h_5 + 4h_6 + 4h_7) \right) \\
 &+ \frac{1}{2} \left(h_{22} \dot{\theta}_1 \dot{\theta}_3 \sin(2\theta_2 + \theta_3) \times (2\dot{\theta}_2 + \dot{\theta}_3) \times h_{19} \right) \\
 &+ \frac{1}{2} \left(h_{11} \sin(\theta_2 + \theta_3 + \theta_4) \times (\dot{\theta}_2 + \dot{\theta}_3 + \dot{\theta}_4)^2 \right) \\
 &+ \frac{1}{2} \left(h_{20} \sin(\theta_2 + \theta_3) \times (\dot{\theta}_2 + \dot{\theta}_3)^2 \times h_{19} \right) \quad (15)
 \end{aligned}$$

$$\begin{aligned}
 c_{21} &= -\frac{1}{8} \times \left(\dot{\theta}_1^2 \sin(2\theta_2 + 2\theta_3) \times (4I_{zz3} + h_8 + 4h_9) \right) \\
 &- \frac{1}{2} \left(h_{15} \sin(\theta_3 + \theta_4) \times (\dot{\theta}_3 + \dot{\theta}_4) \times (2\dot{\theta}_2 + \dot{\theta}_3 + \dot{\theta}_4) \right) \\
 &- \frac{1}{8} \times \left(\dot{\theta}_1^2 \sin(2\theta_2 + 2\theta_3 + 2\theta_4) \times (h_{10} + 4I_{zz4}) \right) \\
 &- \frac{1}{8} \left(\dot{\theta}_1^2 \sin(2\theta_2) \times (4I_{zz2} + h_5 + 4h_6 + 4h_7) \right) \\
 &- \frac{1}{2} \left(h_{22} h_{19} \dot{\theta}_3^2 \sin \theta_3 \times (2\dot{\theta}_2^2 + 2\dot{\theta}_3^2) \right) \\
 &- \frac{1}{2} \left(h_{17} \dot{\theta}_4^2 \sin(\theta_4) \times (2\dot{\theta}_2 + 2\dot{\theta}_3 + \dot{\theta}_4) \right) \\
 &- \frac{1}{2} \left(h_{17} \dot{\theta}_1^2 \sin(2\theta_2 + 2\theta_3 + 2\theta_4) \right) \\
 &- \frac{1}{2} \left(h_{15} \dot{\theta}_1^2 \sin(2\theta_2 + \theta_3 + \theta_4) \right) \\
 &- \frac{1}{2} \left(h_{22} h_{19} \dot{\theta}_1^2 \sin(2\theta_2 + \theta_3) \right) \quad (16)
 \end{aligned}$$

$$\begin{aligned}
 c_{31} &= -\frac{1}{8} \times \left(\dot{\theta}_1^2 \sin(2\theta_2 + 2\theta_3 + 2\theta_4) \times (h_{10} + 4I_{zz4}) \right) \\
 &- \frac{1}{8} \left(\dot{\theta}_1^2 \sin(2\theta_2 + 2\theta_3) \times (4I_{zz3} + h_8 + 4h_9) \right) \\
 &+ \frac{1}{4} \times \left(h_{15} \sin(\theta_3 + \theta_4) \times (\dot{\theta}_1^2 + 2\dot{\theta}_2^2) \right) \\
 &- \frac{1}{2} \left(h_{17} \dot{\theta}_4^2 \sin(\theta_4) \times (2\dot{\theta}_2 + 2\dot{\theta}_3 + \dot{\theta}_4) \right)
 \end{aligned}$$

$$\begin{aligned}
 & + \frac{1}{4} \left(h_{22} h_{19} \sin(\theta_3) \times (\dot{\theta}_1^2 + \dot{\theta}_2^2) \right) \\
 & - \frac{1}{2} \left(h_{17} \dot{\theta}_1^2 \sin(2\theta_2 + 2\theta_3 + \theta_4) \right) \\
 & - \frac{1}{4} \left(h_{15} \dot{\theta}_1^2 \sin(2\theta_2 + \theta_3 + \theta_4) \right) \\
 & - \frac{1}{4} \left(h_{22} h_{19} \dot{\theta}_1^2 \sin(2\theta_2 + \theta_3) \right) \tag{17}
 \end{aligned}$$

$$\begin{aligned}
 c_{41} = & -\frac{1}{8} \times \left(\dot{\theta}_1^2 \sin(2\theta_2 + 2\theta_3 + 2\theta_4) \times (h_{10} + 4I_{zz4}) \right) \\
 & + \frac{1}{4} \left(h_{17} \sin(\theta_4) \times (\dot{\theta}_1 + 2\dot{\theta}_2 + 4\dot{\theta}_2\dot{\theta}_3 + 2\dot{\theta}_3^2) \right) \\
 & + \frac{1}{4} \times \left(h_{15} \sin(\theta_3 + \theta_4) \times (\dot{\theta}_1^2 + 2\dot{\theta}_2^2) \right) \\
 & - \frac{1}{4} \left(h_{17} \dot{\theta}_1^2 \sin(2\theta_2 + 2\theta_3 + \theta_4) \right) \\
 & - \frac{1}{4} \left(h_{15} \dot{\theta}_1^2 \sin(2\theta_2 + \theta_3 + \theta_4) \right) \tag{18}
 \end{aligned}$$

Also, the elements of the gravity vector are below:

$$g_{11} = 0 \tag{19}$$

$$\begin{aligned}
 g_{21} = & -\frac{1}{2} (h_{27} h_{19} \sin(\theta_2 + \theta_3)) - \frac{1}{2} (h_{26} h_{18} \sin(\theta_2)) \\
 & - \frac{1}{2} (h_{25} \sin(\theta_2 + \theta_3 + \theta_4)) \tag{20}
 \end{aligned}$$

$$\begin{aligned}
 g_{31} = & -(\sin(\theta_2 + \theta_3)) \times -\left(\frac{h_{23}}{2} + h_{24} \right) \\
 & - \frac{1}{2} (h_{25} \sin(\theta_2 + \theta_3 + \theta_4)) \tag{21}
 \end{aligned}$$

$$g_{41} = -\frac{1}{2} (h_{25} \sin(\theta_2 + \theta_3 + \theta_4)) \tag{22}$$

τ_{f11} , τ_{f21} , τ_{f31} and τ_{f41} are the components of the friction vector. The dynamic differential equation model of the TLRIP can be expressed by matrix form as follow:

$$\begin{aligned}
 & \begin{bmatrix} M_{11} & M_{12} & M_{13} & M_{14} \\ M_{21} & M_{22} & M_{23} & M_{24} \\ M_{31} & M_{32} & M_{33} & M_{34} \\ M_{41} & M_{42} & M_{43} & M_{44} \end{bmatrix} \begin{bmatrix} \ddot{\theta}_1 \\ \ddot{\theta}_2 \\ \ddot{\theta}_3 \\ \ddot{\theta}_4 \end{bmatrix} + \begin{bmatrix} c_{11} \\ c_{21} \\ c_{31} \\ c_{41} \end{bmatrix} \\
 & + \begin{bmatrix} \tau_{f11} \\ \tau_{f21} \\ \tau_{f31} \\ \tau_{f41} \end{bmatrix} + \begin{bmatrix} g_{11} \\ g_{21} \\ g_{31} \\ g_{41} \end{bmatrix} = \begin{bmatrix} \tau \\ 0 \\ 0 \\ 0 \end{bmatrix} \tag{23}
 \end{aligned}$$

In order to examine the effects of the inertia of the vertical arms in the TLRIP, the dynamic equations of the TLRIP were solved in different inertia cases. In the first case, the inertia tensor of the links is neglected in the dynamic model. In the second case, only the component I_{zz} of the inertia tensor is considered for each link. In the last case, full inertia tensor iI is taken into consideration in the dynamic model. Figure 2 shows the joints' positions of the TLRIP obtained by the three different dynamic simulation models for the initial condition of, $\theta_1 = 0^\circ$, $\theta_2 = 20^\circ$, $\theta_3 = 30^\circ$ and $\theta_4 = 40^\circ$. The simulation results of the dynamic equations with only the component I_{zz} of the inertia tensor and the full inertia tensor iI are almost the same in low velocities of

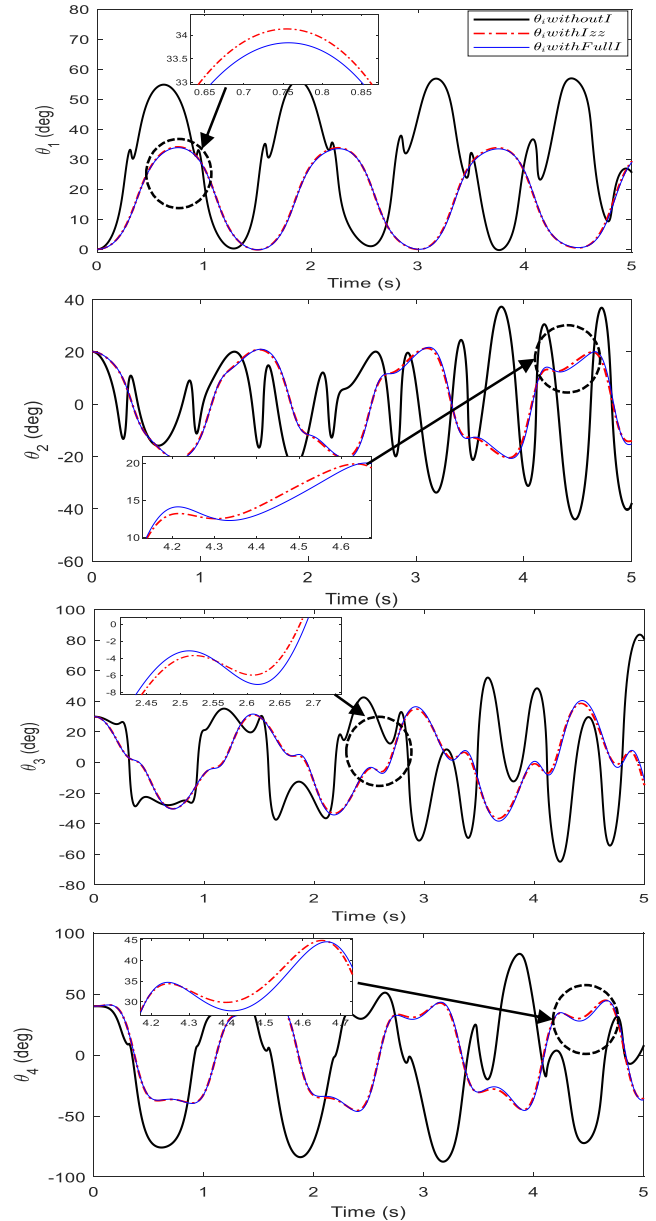


FIGURE 2. Comparison of the joint positions of the TLRIP under different usages of the inertia.

the arms. On the other hand, the dynamic model where the inertia is neglected is not acceptable. In order to have a more simplified dynamic model in the equilibrium control of the TLRIP, only the component I_{zz} of the inertia tensor can be employed. On the other hand, the accurate dynamic model in swing-up control of the TLRIP is very important to compute the total energy of the pendulum. Therefore, the full inertia tensor iI should be taken into consideration in the dynamic model of the pendulum with a complex structure. In order to compare the analytic mathematical model, the numeric dynamic model of the TLRIP was developed by using the MATLAB/SimMechanics toolbox.

The MATLAB/SimMechanics model of the TLRIP is shown in Figure 3. In the simulations, the first horizontal arm

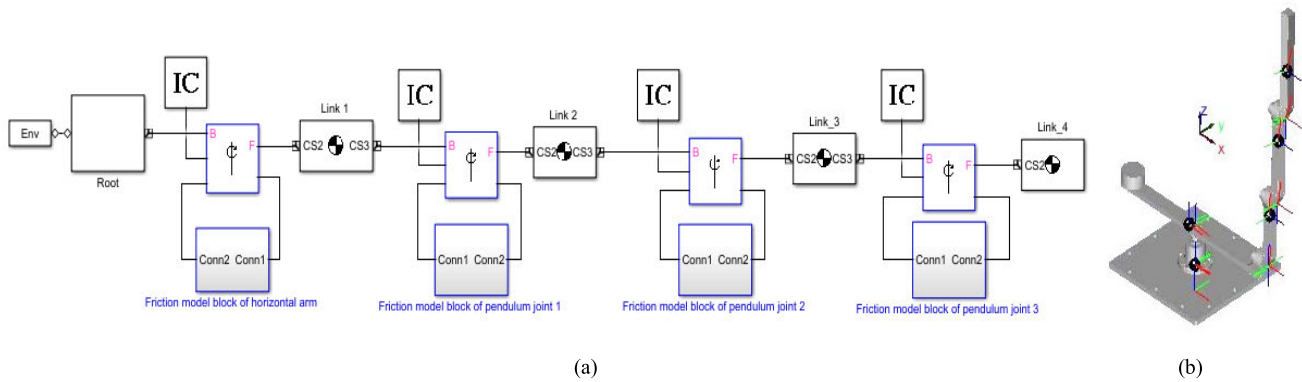


FIGURE 3. a) MATLAB/SimMechanics model of the TLRIP, b) solid model of the TLRIP.

angle position is fixed at zero position. Therefore, only the vertical links joints (θ_2, θ_3 and θ_4) are considered for friction estimation analysis. In this way, the effect of friction on the shaft of the motor-driven system on the joint dynamics of the pendulum is prevented. The initial conditions of pendulums' joint positions (θ_2, θ_3 and θ_4) of MATLAB/SimMechanics, mathematical model and experience are chosen as follows, $\theta_2 = 20.56^\circ, \theta_3 = 32.21^\circ$ and $\theta_4 = 45^\circ$. The obtained results from both the MATLAB/SimMechanics model and the mathematical model match exactly. Figure 4 illustrates a comparison of the three joint positions obtained from simulation (analytic mathematical model and the SimMechanics model without frictions) and experimental results. As can be

seen from the figure, position errors of the joints in TLRIP occurred highly since joint friction dynamics are ignored. Therefore, the friction models should be determined explicitly to obtain the most accurate dynamic model of the pendulums. The friction estimation models in the literature will be described in the next section.

III. FRICTION ESTIMATION MODELS

The joint frictions are dependent on many physical parameters, such as position, velocity and acceleration of the joints [1]. The changes in the positions, velocities and the accelerations of the pendulums can change the friction's characteristics in a complex manner [13]. The dynamic behavior of the joints' frictions is simulated with the different models in the existing literature. Most of these models are defined by friction coefficients. Therefore, it is necessary to develop an accurate friction model to estimate the friction's coefficients in the joints in accordance with the dynamic behavior of positions, velocities and accelerations. NCFM, LFM, and NLFM estimation models were given in the papers [6], [17], [19]–[21]. To estimate the constant friction coefficients in the pendulum's joints of the TLRIP, different friction estimation models (NCFM, LFM, and NLFM) were examined in detail in [10]. These friction models consist of different important components. Each component takes care of certain aspects of the friction force in the joints [14], [15].

Mostly used friction model in the literature is the generalized static friction model which depends only on the velocity (v). It describes only the steady-state behavior of the friction force F_f in the sliding regime and it is given the equation below [16].

$$F_f = \sigma_2 v + \text{sign}(v) \left(F_c + (F_s - F_c) \exp \left(- \left| \frac{v}{V_s} \right|^\delta \right) \right) \quad (24)$$

The first term represents the viscous friction force and the second term equals the Stribeck effect. F_s, F_c, V_s, δ and σ_2 are the static force, the Coulomb force, the Stribeck force, the shape factor and the viscous friction coefficient, respectively. this model has the discontinuity at velocity

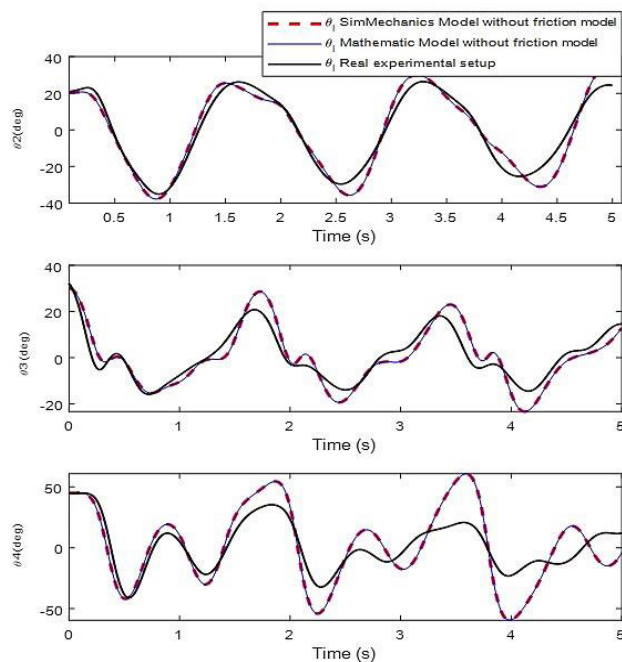


FIGURE 4. Comparison of the joint positions obtained from the mathematical model without frictions, SimMechanics model without frictions and the real experimental setup.

reversal which causes errors or even instability during friction compensation.

A. NON-CONSERVATIVE FRICTION MODEL

NCFM is a classical friction model. It has been used in the first works related to the control of pendulums to estimate the friction in the joints, which based only on one type of friction coefficient [17]. The non-conservative torques due to natural damping of the pendulums called viscous friction torque and it is introduced through Rayleigh's dissipation function $\mathcal{D}(\dot{\theta}_i)$ [6]. The non-conservative friction torque is given in equation (25).

$$F_v = \frac{d\mathcal{D}(\dot{\theta}_i)}{d\dot{\theta}_i} = \frac{d}{d\dot{\theta}_i} \left(\frac{1}{2} \overline{C}_p \dot{\theta}_i^2 \right) = \overline{C}_p \dot{\theta}_i \quad (25)$$

where \overline{C}_p is the viscous friction coefficient and $\dot{\theta}_i$ is the angular velocity of the i -th pendulum.

B. LINEAR FRICTION MODEL

LFM is a combination of the Viscous friction presented in the non-conservative model and another type of friction called Coulomb friction [18], the LFM, which is presented by equation (26).

$$F_l = F_v + F_c \quad (26)$$

where F_c is the Coulomb frictions and F_v is the viscous friction torque which is proportional to the angular velocity $\dot{\theta}_i$, and given by equation (27) [19].

$$F_v = B_i \dot{\theta}_i \quad (27)$$

where B_i are the constant viscous coefficients. The Coulomb friction is proportional to the normal load force N_f which is derived as follows:

$$N_f = m\omega^2 l + mg \cos(\theta) \quad (28)$$

l is the distance from the pendulum rotation center to the mass center.

The pendulum parameters are given in Figure 5. The Coulomb frictions F_c is given by equation (29).

$$F_c = C_i \operatorname{sgn}(\dot{\theta}_i) \cdot (m \dot{\theta}_i^2 + mg \cos(\theta_i)) \quad (29)$$

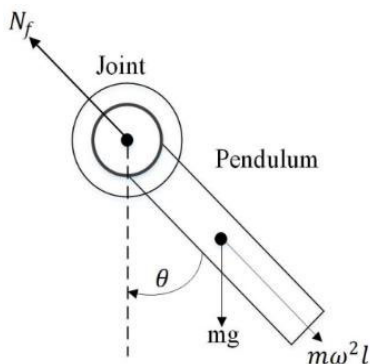


FIGURE 5. Pendulum parameters.

where C_i are the dynamic friction coefficients and $\operatorname{sgn}(\cdot)$ is the signum function.

C. NON-LINEAR FRICTION MODEL

The new researches in the field of friction estimation have found that the frictions in the joints can be affected by several factors such as temperature, force/torque, position, velocity and acceleration. Since friction has a complex nonlinear nature [20], the LFM becomes an oversimplified model in friction structure. The TLRIP system can move in trajectories which have high and suddenly changing, position speed, acceleration and jerk. The LFM cannot cover these characteristics, especially at sudden motion reversal [21]. Therefore, the NLFM reflects a better description of the joint friction characteristics. This model can be described in the following nonlinear equations (30) [22].

$$\tau_f = f_o + f_c \operatorname{sgn}(\dot{\theta}_i) + f_v \dot{\theta}_i + f_a \operatorname{atan}(f_b \dot{\theta}_i) \quad (30)$$

where f_o the zero-drift error of friction torque, f_c is the Coulomb friction coefficient, f_v is the viscous friction coefficient. $f_a \operatorname{atan}(f_b \dot{\theta}_i)$ present the experimental friction in zero velocity behavior, which f_a and f_b are the experimental friction coefficients. $\dot{\theta}_i$ is the angular velocity, sgn is the signum function and atan is the arctangent function. In fact, it appears that this nonlinear friction model is derived from the generalized friction model (equation (24)). The only difference between the two equations (24 and 30), the third term in equation 24 is modelled with the first and fourth term in equation (30). The reason for using the arctangent function in equation (30) is to overcome the discontinuity at zero velocity equation (24).

D. ADAPTIVE FRICTION MODEL

ZB Hazem et al. [1] developed the AFEM to estimate the variable joint frictions in TLRIP. More details about the friction estimation model can be found in [1]. This model takes into consideration the experimental joint velocity and accelerations. These accelerations can be grouped into three categories (low, medium and high). The adaptive friction coefficients are tuned using pattern search algorithm and these estimated coefficients were verified experimentally.

In the next section, the proposed Neuro-Fuzzy friction estimation models will be presented.

IV. IMPLEMENTATION OF NEURO-FUZZY FRICTION ESTIMATION MODEL

In this work, a fuzzy logic inference system is developed to estimate the friction coefficients in the pendulum joints of the TLRIP. For each joint, an FLC (Fuzzy Logic Controller) implemented to estimate the friction coefficients, Figure 6 depicts the implementation of the FLC in the joints of the TLRIP. Two inputs of FLC are the joints velocities and accelerations. The typical steps in developing the FLC system involve fuzzification, rule formation and defuzzification is explained briefly in this section.

TABLE 4. Selection of range for the input and output variables.

Joints	Input variables				Output variables			
	Velocity	Ranges	Acceleration	Ranges	B and C	B-Ranges	C-Ranges	
Joint 2	VS	[0 95]	NH	[-6000 -2300]	VH	[0 2,53.10 ⁻⁴]	[0 2,601.10 ⁻⁴]	
	S	[85 280]	NM	[-5000 -200]	H	[1,263. 10 ⁻⁴ 4,778. 10 ⁻⁴]	[1,073 .10 ⁻⁴ 5,121.10 ⁻⁴]	
	M	[200 600]	ZE	[-1000 1000]	M	[4,086. 10 ⁻⁴ 5,916. 10 ⁻⁴]	[4,087.10 ⁻⁴ 6,139.10 ⁻⁴]	
	F	[450 920]	PM	[-200 6500]	L	[5,396. 10 ⁻⁴ 8,837. 10 ⁻⁴]	[5,449.10 ⁻⁴ 9,378.10 ⁻⁴]	
	VF	[690 1000]	PH	[3800 8000]	VL	[7,457 . 10 ⁻⁴ 10 . 10 ⁻⁴]	[7,624.10 ⁻⁴ 10 . 10 ⁻⁴]	
Joint 3	VS	[0 110]	NH	[-14000 -8177]	VH	[1. 10 ⁻⁶ 3,236. 10 ⁻⁶]	[1. 10 ⁻⁶ 2,516. 10 ⁻⁶]	
	S	[69 400]	NM	[-10880-2483]	H	[1,757. 10 ⁻⁶ 5,254. 10 ⁻⁶]	[1,59. 10 ⁻⁶ 4,043. 10 ⁻⁶]	
	M	[280 800]	ZE	[-3546 375.9]	M	[4,624. 10 ⁻⁶ 6,288. 10 ⁻⁶]	[3,416. 10 ⁻⁶ 4,66. 10 ⁻⁶]	
	F	[590 1200]	PM	[-611.2 10610]	L	[5,814. 10 ⁻⁶ 9,344. 10 ⁻⁶]	[4,23. 10 ⁻⁶ 6,61. 10 ⁻⁶]	
	VF	[900 1300]	PH	[7793 22330]	VL	[7,688. 10 ⁻⁶ 1,002. 10 ⁻⁵]	[5,56. 10 ⁻⁶ 7. 10 ⁻⁶]	
Joint 4	VS	[0 355]	NH	[-2.3. 10 ⁴ -1,457. 10 ⁴]	VH	[0 3,232. 10 ⁻⁶]	[0 2,769. 10 ⁻⁶]	
	S	[138 669]	NM	[-1,84. 10 ⁴ -6242]	H	[2,057. 10 ⁻⁶ 5,252. 10 ⁻⁶]	[1,688. 10 ⁻⁶ 4,55. 10 ⁻⁶]	
	M	[510 1337]	ZE	[-7860 -2180]	M	[4,624. 10 ⁻⁶ 6,287. 10 ⁻⁶]	[3,782. 10 ⁻⁶ 5,233. 10 ⁻⁶]	
	F	[1075 2043]	PM	[-3610 1,264. 10 ⁴]	L	[5,815. 10 ⁻⁶ 8,942. 10 ⁻⁶]	[4,781. 10 ⁻⁶ 7,561. 10 ⁻⁶]	
	VF	[1608 3026]	PH	[8566 1,909. 10 ⁴]	VL	[7,687. 10 ⁻⁶ 1,002. 10 ⁻⁵]	[6,32. 10 ⁻⁶ 8, 10 ⁻⁶]	

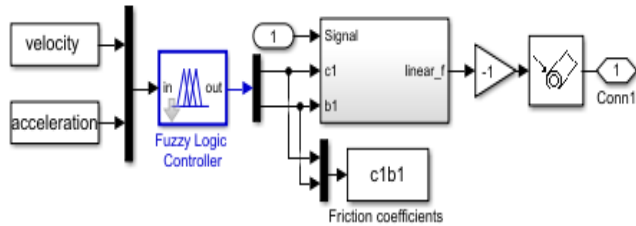


FIGURE 6. Simulink implementation of FLC in each joint of the TLRIP.

The input variables such as velocities and accelerations are suitably partitioned and converted into linguistic variables, as following (NL-negative medium, Z-zero, PM-positive medium, PH- positive high, VS- very slow, S-slow, F-fast, VF- very fast, M- medium). The output variables (friction coefficients of the models) are partitioned and represented as fuzzy sets with linguistic terms as following (M- medium, L-large, VL-very large, H- high and VH- very high). The maximal absolute experimental velocities and acceleration of the pendulums' joints are 1000 deg/s and 8000 deg/s² respectively. The membership functions and ranges of the input variables are obtained based on the experimental velocities and accelerations classification. Also, the membership functions and ranges of the output variables is obtained relatively from friction coefficients of the Adaptive Friction Estimation Model (AFEM) given in Tables 7, 8, and 9 in section 5. The fuzzy rules are the most important part of the entire method, which affect the output results crucially. They are set based on the experimental velocities and acceleration classification knowledge and results obtained theoretically by the AFEM for each class. An example of the range selections for the input and output variables in LFM are shown in Table 4. Gaussian membership functions were used for graphical inference of the input and the output variables. As an example of many membership functions of the joints in the friction models used here, the membership functions of the first joint in LFM are illustrated in Figure 7. A fuzzy rule

is a standard form of expressing knowledge based on the logic of IF and Then functions. A set of rules have been constructed based on the input variables (velocities and accelerations) and output variables (friction coefficients) for the three joints of TLRIP. The fuzzy rules used here are given in Table 5. The FLC rules for each of pendulum joint were obtained based on the experimental results from velocities and accelerations in AFEM [1].

TABLE 5. (a). FLC rules for pendulums' joints.

Vel Acc	VS	S	M	F	VF
F.Cof	BI CI	BI CI	BI CI	BI CI	BI CI
NH	VH H	VH VH	H VH	M H	L M
NM	VH H	H VH	H H	M M	VL L
ZE	VH VH	H H	M H	L M	VL L
PM	VH VH	H H	M H	L L	VL VL
PH	H H	M M	L H	VL L	VL VL

The defuzzification is the conversion of a fuzzy quantity to a crisp value. The centroid method was applied for defuzzification. Figure 8 shows the FLC surface relationship between velocities, accelerations and friction coefficients of the three joints in LFM.

The friction coefficients obtained by the fuzzy logic inference system was trained by using a Radial Basis Function Artificial Neural Network (RBANN). The sampling rate is chosen as 1khz (sampling time) for the 40s (experiment test time) the velocities and accelerations inputs data are 40000 samples, respectively. the RBFNN method produces better training of a big number of data. RBFNN have the advantages of an easy design (just three-layer architecture), good generalization, and high tolerance of input noises and the ability of online learning. RBFNNs are simpler than other networks existing in the literature [23], [24].

This network uses the Bayesian Regularization (BR) algorithm [25] to treat the joint velocities and accelerations as inputs and the resultant frictions coefficients of fuzzy logic

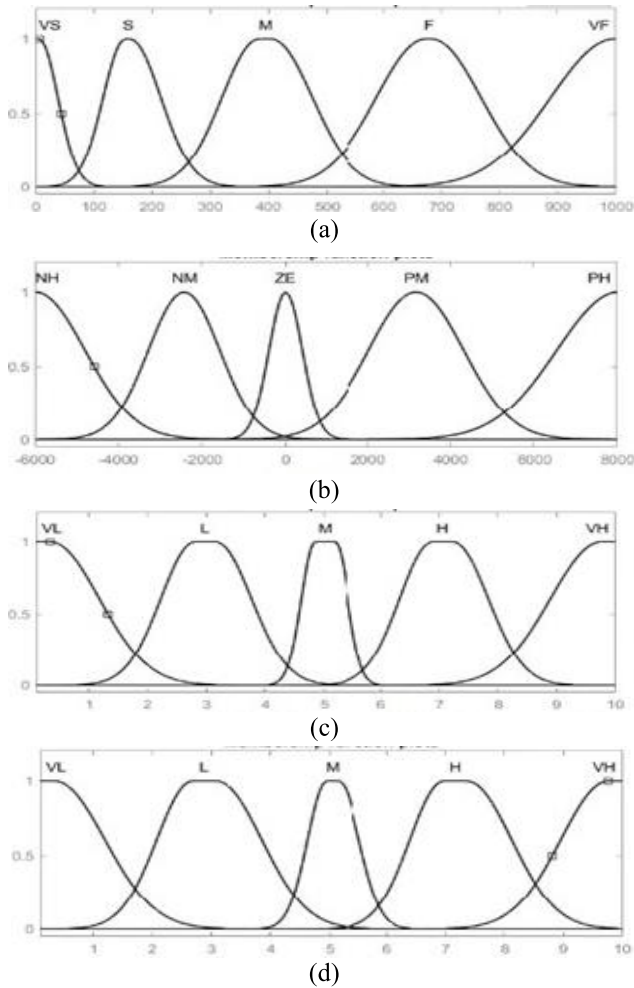


FIGURE 7. FLC membership functions of the first joint in LFM. (a) Velocity membership functions. (b) Acceleration membership functions. (c) Friction coefficient (B) membership functions. (d) Friction coefficient (C) membership functions.

as targets. The Bayesian Regularization (BR) algorithm performance is dependent by the minimal Means Squared Error (MSE). The RBANN model expressed by two neurons in the input layer, 10 neurons in the hidden layer, and two neurons in the output layer. The RBANN model is developed in each pendulum's joint of the TLRIP. Figure 9 illustrates the block diagram of the NFFEM architecture for the TLRIP. The filter seen in figures 9 and 10 is an IIR (Infinite Impulse Response) filter which is explained in section V-B. Where θ_i , $\dot{\theta}_i$ and $\ddot{\theta}_i$ are the joints' angles positions, the angular velocities and the angular accelerations of the i -th pendulums.

The experimental and simulation results will be discussed in the next section.

V. EXPERIMENTAL SETUP AND RESULTS

A. DATA COLLECTION

The horizontal arm of the TLRIP is driven by a direct drive brushless DC torque motor (Type: TMH-130-050-NC). In this type of motor, since there is no use of transmission or

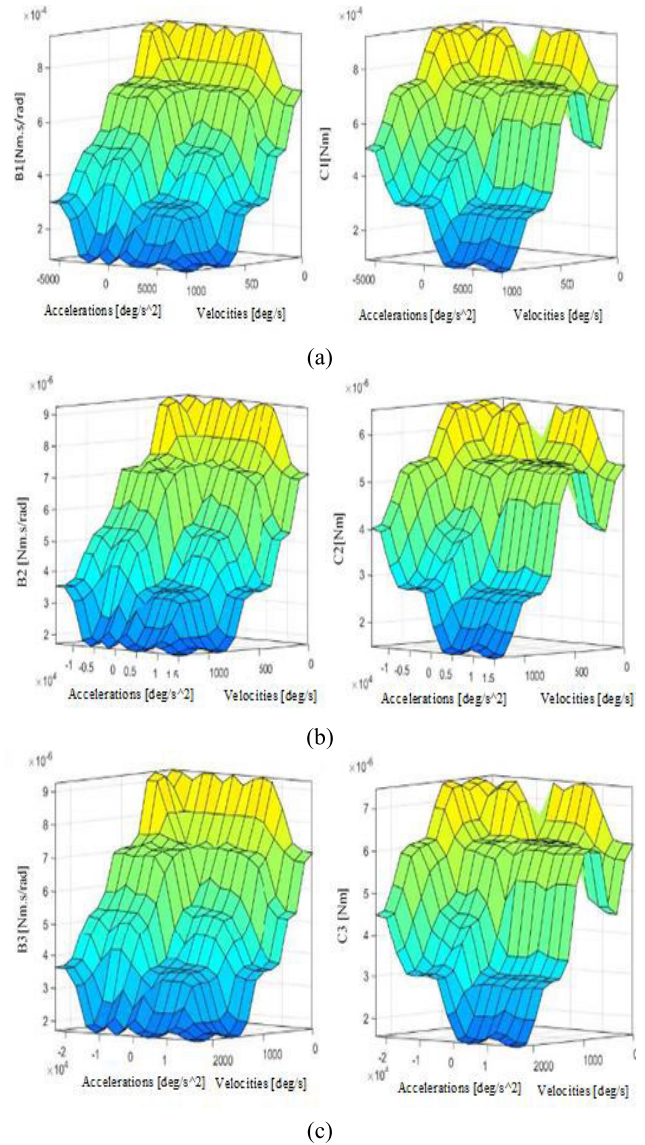


FIGURE 8. FLC surface in LFM for pendulums joints. (a) Joint 2 (b) Joint 3 (c) Joint 4.

gearbox, the frictions in the horizontal arm can be considered negligible. During the collection of the experimental data, the arm joint θ_1 is fixed at zero position. The pendulums' angles (θ_2 , θ_3 and θ_4) are measured with three encoders having a resolution of 2048 pulses per revolution. The signals obtained from the encoder passes through the slip ring mounted in the joints. A dSPACE-DS1103 controller board treats the received signals from the encoders. The friction in the joints of the TLRIP depends on their velocities and the accelerations. In this case, the friction coefficients of the AFEM and NFFEM should be determined experimentally. The initial positions of the pendulums will be taken in cases with the value of θ_2 at 180 degrees along with θ_3 and θ_4 at an angle of 0 degrees. The experimental hardware configuration is shown in Figure 10. In this work, the frequency counting technique [26] was used to obtain velocity and acceleration

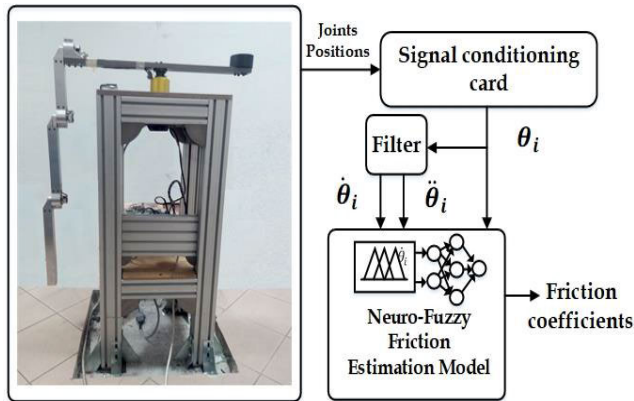


FIGURE 9. Block diagram of the NFFEM architecture for the TLRIP.

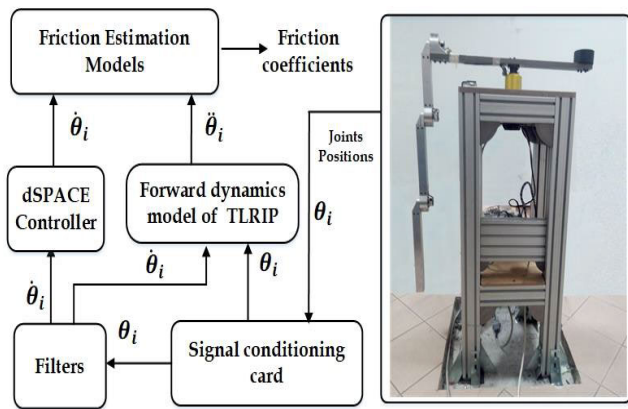


FIGURE 10. Block diagram of the experimental hardware configuration structure.

from an incremental encoder. This technique is useful for medium and high speeds but degrades in performance at low speed since the relative error increases at low speed. For this reason, a second-order IIR filter [27], [28] was used to smooth the signal.

B. RESULTS AND DISCUSSION

In the AFEM, the Pattern Search (PS) method was used to optimize the frictions coefficients. The PS method allows the optimization of a number of parameters at the same time [29]. The simulation results obtained from the AFEMs and NFFEMs based on NCFM, LFM and NLFM were compared with the experimental results. For each joint, position RMSEs between these simulation and experimental results were calculated.

1) AFEM

Table 6 presents the classification of joints accelerations and their values into different groups as follows: High [0-7s], medium [7-14s] and low [14-40s] for joint of the first pendulum; high [0-6s], medium [6- 16s] and low [16-40s] for joint of the second pendulum 2; low [0-1.3s], high [1.3- 4.5s], medium [4.5-13s] and low [13-30s] for joint of the Third

TABLE 6. Classification of joints accelerations.

Joint 2				
Time [s]	Positions value [Deg]		Accelerations value [Deg/s ²]	
	Max	Min	Max	Min
[0-7]	134.2969	91.9775	$6.911 \cdot 10^3$	$4.2371 \cdot 10^3$
[7 -14]	14.3701	8.7451	$1.115 \cdot 10^3$	$0.9755 \cdot 10^3$
[14 - 40]	3.7793	3.6914	59.0392	56.8847
Joint 3				
[0-6]	159.5215	128.6279	$1.242 \cdot 10^4$	$1.1017 \cdot 10^4$
[6-16]	77.1680	53.7891	$6.160 \cdot 10^3$	$4.9842 \cdot 10^3$
[16 -40]	2.3730	2.1094	63.8500	52.9298
Joint 4				
[0- 1.3]	489.6387	120.1465	$1.709 \cdot 10^4$	$1.5173 \cdot 10^4$
[1.3- 4.5]	877.2803	489.6387	$1.468 \cdot 10^4$	$0.8899 \cdot 10^4$
[4.5 -13]	1.2357	0.8773	$8.633 \cdot 10^3$	$6.2568 \cdot 10^3$
[13 - 30]	$1.13 \cdot 10^3$	$1.01 \cdot 10^3$	$3.488 \cdot 10^3$	$3.3282 \cdot 10^3$

TABLE 7. Adaptive friction coefficients obtained by NCFM.

Time of Joint 2 [s]	[0-7]	[7 -14]	[14 - 40]	
C_p [Nm.s/rad]	0.0040	0.0033	0.0335	
Time of Joint 3 [s]	[0 - 6]	[6 -16]	[16 - 40]	
C_p [Nm.s/rad]	2.4410^{-4}	0.0015	0.001514	
Time of Joint 4 [s]	[0 -1.3]	[1.3-4.5]	[4.5-13]	[13 - 40]
C_p [Nm.s/rad]	0.00100	7.4710^{-5}	1.10^{-4}	$7.3 \cdot 10^{-6}$

TABLE 8. Adaptive friction coefficients obtained by LFM.

Time of Joint 2 [s]	[0 - 7]	[7 - 14]	[14 - 40]	
B_i [Nm.s/rad]	0.0015	0.0037	0.0314	
C_i [Nm]	0.0209	0.0429	0.0174	
Time of Joint 3 [s]	[0 to 6]	[6 to 16]	[16 - 40]	
B_i [Nm.s/rad]	0.0030	0.0018	0.001497	
C_i [Nm]	$2.4 \cdot 10^{-4}$	0.00277	$1.000 \cdot 10^{-4}$	
Time of Joint 4 [s]	[0 - 1.3]	[1.3- 4.5]	[4.5 - 13]	[13 - 30]
B_i [Nm.s/rad]	5.4910^{-5}	$7.4 \cdot 10^{-5}$	$8.6 \cdot 10^{-5}$	$8.7 \cdot 10^{-5}$
C_i [Nm]	0.0050	$6.3 \cdot 10^{-4}$	$1.5 \cdot 10^{-4}$	$1.5 \cdot 10^{-4}$

pendulum 3. Tables 7, 8, and 9 present the adaptive friction coefficients using the NCFM, LFM, and NLFM, respectively. Where C_p is the viscous friction coefficient for each pendulum joint of the ANCFM. B_i and C_i are the constants of Viscous and Coulomb friction coefficients for each pendulum joint of the ALFM. Also, the ANLFM depend by: f_o is the zero-drift error of friction torque, f_c is the Coulomb friction coefficient, f_v is the viscous friction coefficient. f_a and f_b are the experimental friction coefficients of each pendulum joint.

2) NFFEM

Figure 11, 12 and 13 illustrate the friction coefficients obtained by the: Neuro-Fuzzy Non-Conservative Friction Model (NFNCFM), Neuro-Fuzzy Linear Friction Model (NFLFM) and Neuro-Fuzzy Non-Linear Friction Model (NFNLFM) for the joints of the TLRIP, respectively. Figure 14 illustrates the angular position comparison between experimental and NFNLFM simulation results. As can be seen from the figure, a high estimation performance is produced with the use of NFNLFM for each joint.

TABLE 9. Adaptive friction coefficients obtained by NFLFM.

Time of Joint 2 [s]	[0 - 7]	[7 - 14]	[14 - 40]	
f_o [Nm]	$9.03 \cdot 10^{-5}$	0.0040	$1.11 \cdot 10^{-4}$	
f_c [Nm]	$2.3530 \cdot 10^{-4}$	0.2421	0.01534	
f_v [Nm.s/rad]	$3.91191 \cdot 10^{-6}$	$3.60 \cdot 10^{-6}$	$3.51961 \cdot 10^{-5}$	
f_a [Nm]	$2.8946 \cdot 10^{-6}$	$1.43 \cdot 10^{-2}$	$9.1137 \cdot 10^{-5}$	
f_b [Nm]	$6.4761 \cdot 10^{-5}$	$8.8510 \cdot 10^{-5}$	$2.9317 \cdot 10^{-7}$	
Time of Joint 3 [s]	[0-6]	[6- 16]	[16 - 40]	
f_o [Nm]	$6.5109 \cdot 10^{-5}$	$1.61 \cdot 10^{-4}$	0.00843	
f_c [Nm]	$9.7363 \cdot 10^{-5}$	$8.1410 \cdot 10^{-5}$	0.01538	
f_v [Nm.s/rad]	$1.1790 \cdot 10^{-5}$	$1.54 \cdot 10^{-6}$	0.00585	
f_a [Nm]	$2.3295 \cdot 10^{-4}$	$2.7210 \cdot 10^{-4}$	$2.23 \cdot 10^{-5}$	
f_b [Nm]	$7.7406 \cdot 10^{-5}$	$3.58 \cdot 10^{-5}$	$1.49 \cdot 10^{-4}$	
Time of Joint 4 [s]	[0 - 1.3]	[1.3 - 4.5]	[4.5 - 13]	[13-30]
f_o [Nm]	0.0454	0.0468	0.0085	$1.3362 \cdot 10^{-5}$
f_c [Nm]	0.2768	0.2541	$4.32 \cdot 10^{-5}$	$9.7910 \cdot 10^{-5}$
f_v [Nm.s/rad]	$8.08 \cdot 10^{-4}$	0.0028	$4.6348 \cdot 10^{-5}$	$2.1810 \cdot 10^{-4}$
f_a [Nm]	0.7500	0.36377	$1.2 \cdot 10^{-5}$	$1.09 \cdot 10^{-4}$
f_b [Nm]	$3.55 \cdot 10^{-4}$	$7.9510 \cdot 10^{-4}$	0.0077	$1.85 \cdot 10^{-4}$

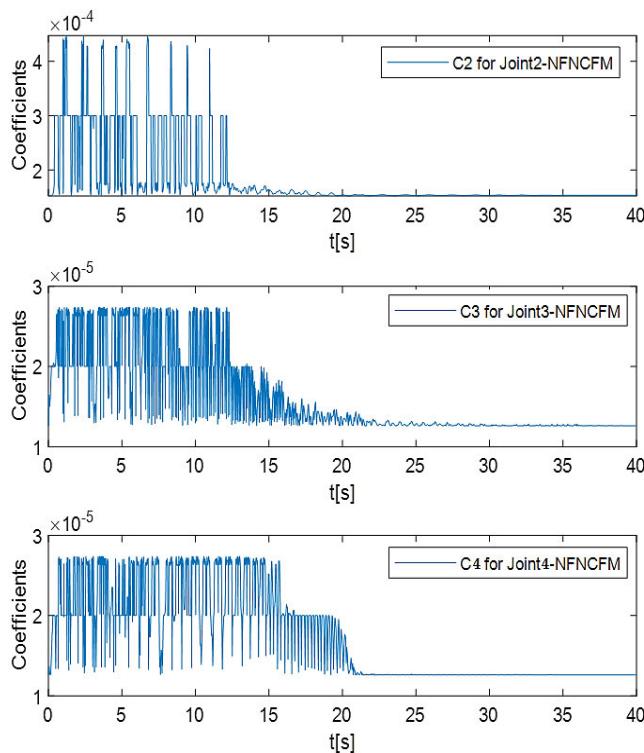


FIGURE 11. Friction coefficients (C = [Nm]) obtained by NFNCFM for pendulums joints.

The joint position RMSEs between the simulation and experimental results of the AFEM and NFFEM were calculated. For comparison purpose, these position RMSEs are given in Table 10. According to the calculated position RMSEs, the NFNLFM produces more accurate results than

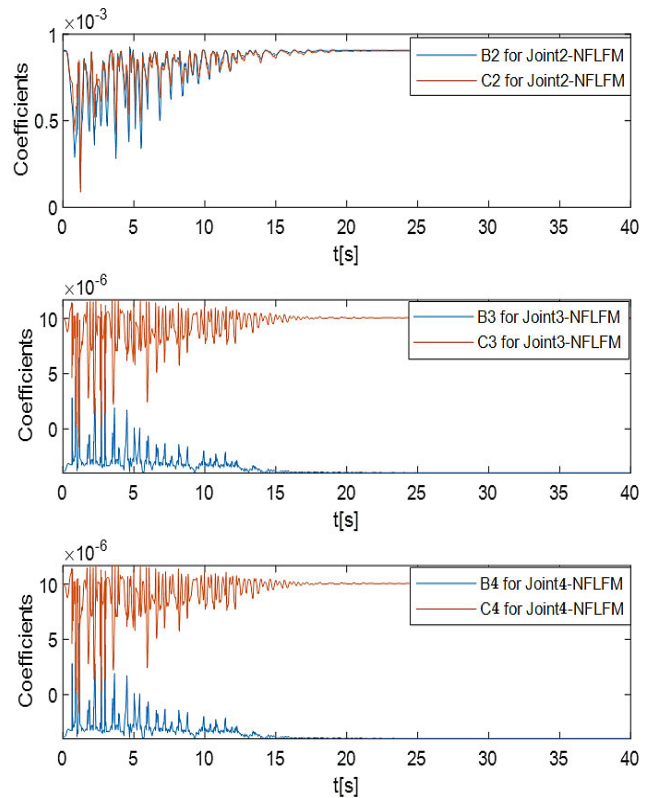


FIGURE 12. Friction coefficients (C = [Nm] and B = [Nm.s/rad]) in NFLFM for pendulums joints.

TABLE 10. Position RMSEs in AFEMs and NFFEMs.

JOINTS FRICTION MODELS		JOINT 2	JOINT 3	JOINT 4
ADAPTIVE FRICTION COEFFICIENTS	ANCFM	0.1397	1.8105	0.6995
	ALFM	0.1127	1.8032	0.6743
	ANLFM	0.0983	0.1115	0.6248
NEURO-FUZZY COEFFICIENTS	NFNCFM	0.1259	0.8105	0.5480
	NFLFM	0.0987	0.1794	0.4372
	NFNLFM	0.0829	0.0986	0.3304

TABLE 11. Comparison in terms of RMSE Percentage between NFNLFM and other friction models.

FRICTION MODELS	RMSE PERCENTAGES BETWEEN NFNLFM AND OTHER FRICTION MODELS		
	JOINT 2	JOINT 3	JOINT 4
ANCFM	40.65 %	94.55%	52.76%
ALFM	26.44%	94.53%	51.00%
ANLFM	15.66%	11.56%	47.11%
NFNCFM	34,15%	87,83%	39,70%
NFLFM	16,00%	45,03%	24,42%

the ANCFM, ALFM, ANLFM, NFNCFM, and NFLFM. In order to see the NFNLFM performance compared with other friction models, percentages of position RMSEs were computed for each joint and they are given in Table 11. Considering the RMSEs of position in all joints, NFNLFM between 11.56 of percentage and 94.55 of percentage yields better results.

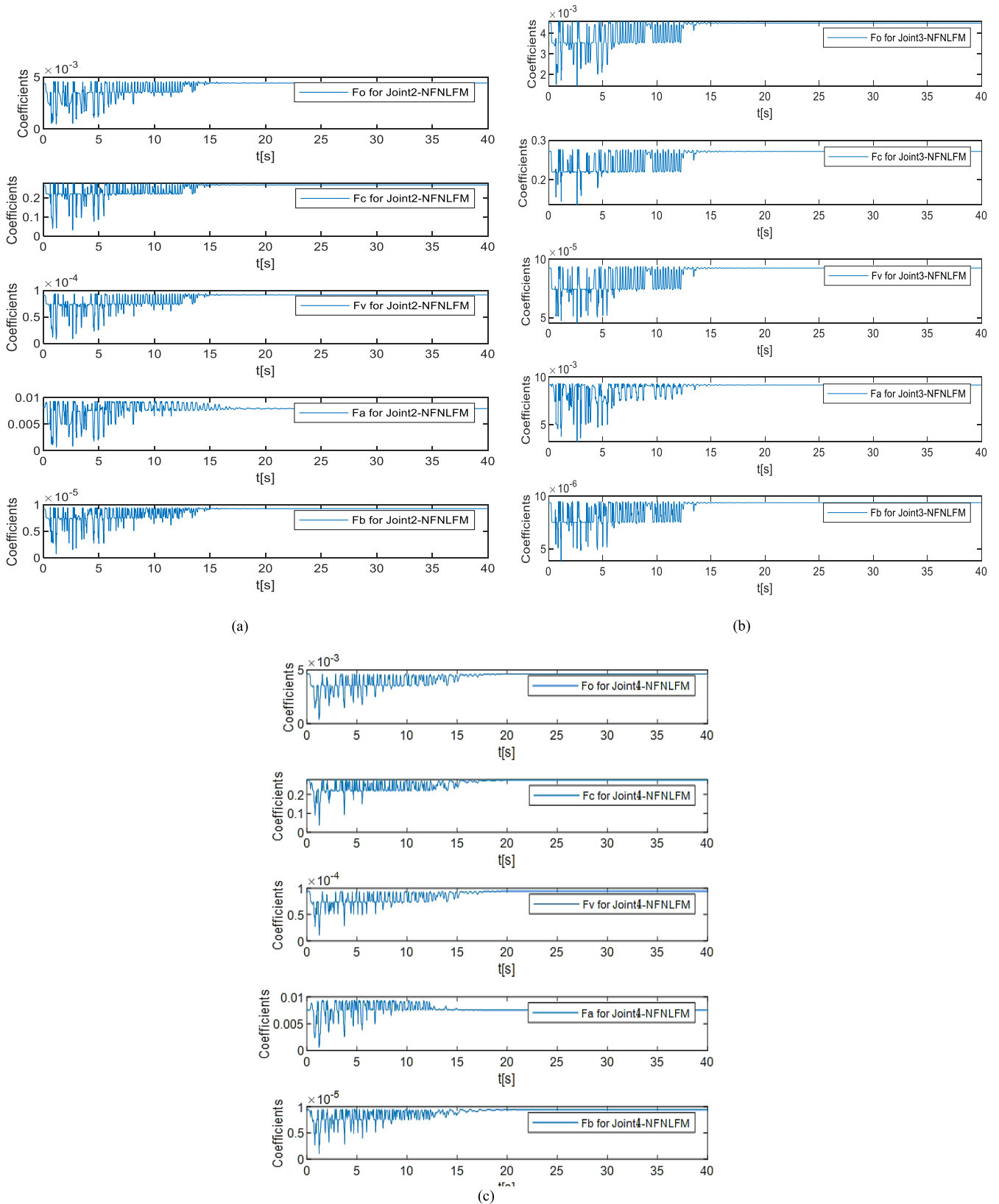


FIGURE 13. Friction coefficients in NFNLFM (f_o , f_c , f_a , f_b = [Nm] and f_v [Nm · s/rad]): (a) Joint 2, (b) Joint 3 and (c) Joint 4.

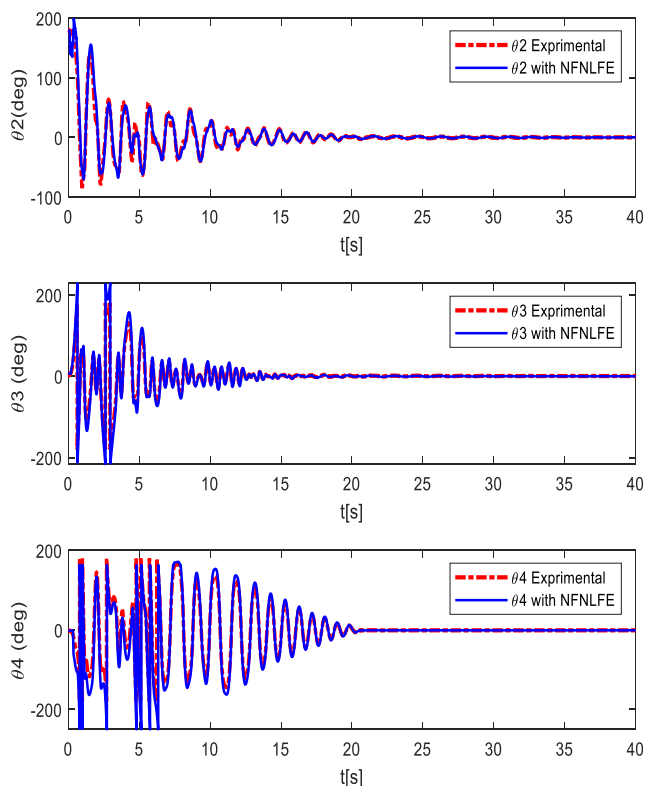


FIGURE 14. Angular position comparison between experimental and NFNLFM simulation results.

VI. CONCLUSION

In this paper, a novel NFFEMs is developed based on NCFM, LFM and NLFM to estimate the joint friction coefficients in the TLRIP system. The simulation results obtained from NFFEMs were compared with AFEMs. For wide ranges of velocity and acceleration of joints, the variable friction coefficients were estimated with the NFFEMs and AFEMs. All of the friction models were verified and compared using the calculated position RMSEs. According to the performance comparison, the NFNLFM in NFFEMs produced the best results for all joints of the TLRIP. In future works, the fuzzification ranges and rules of the NF system will be tuned with evolutionary algorithms to enhance the estimation performance of the NFFEMs. Furthermore, more inputs such as jerks and snaps of the joints will be applied to the NF system and the TLRIP system will be controlled using the proposed friction models.

ACKNOWLEDGMENT

The authors would like to thank The Presidency of Turks Abroad and Related Communities for the doctorate scholarship. They would also like to thank the Scientific Research Projects Coordination Unit of Kocaeli University for the experimental setup support.

REFERENCES

[1] Z. B. Hazem, M. Javad Fotuhi, and Z. Bingul, "A comparative study of the friction models with adaptive coefficients for a rotary triple inverted pendulum," in *Proc. 6th Int. Conf. Control Eng. Inf. Technol. (CEIT)*, Oct. 2018, pp. 25–27.

[2] S. Awatar, N. King, T. Allen, I. Bang, M. Hagan, D. Skidmore, and K. Craig, "Inverted pendulum systems: Rotary and arm-driven—a mechatronic system design case study," *Mechatronics*, vol. 12, no. 2, pp. 357–370, Mar. 2002.

[3] M. Ramírez-Neria, H. Sira-Ramírez, R. Garrido-Moctezuma, and A. Luviano-Juárez, "Linear active disturbance rejection control of underactuated systems: The case of the furuta pendulum," *ISA Trans.*, vol. 53, no. 4, pp. 920–928, Jul. 2014.

[4] M. Antonio-Cruz, R. Silva-Ortigoza, C. A. Merlo-Zapata, M. G. Villarreal-Cervantes, D. Munoz-Carrillo, and V. M. Hernandez-Guzman, "Modeling and construction of a furuta pendulum prototype," in *Proc. Int. Conf. Mechatron., Electron. Automot. Eng.*, Nov. 2014, pp. 98–103.

[5] O. García-Alarcón, S. Puga-Guzmán, and J. Moreno-Valenzuela, "On parameter identification of the furuta pendulum," *Procedia Eng.*, vol. 35, pp. 77–84, Jan. 2012.

[6] J. Á. Acosta, "Furuta's pendulum: A conservative nonlinear model for theory and practise," *Math. Problems Eng.*, vol. 2010, Mar. 2010, Art. no. 742894.

[7] D. Park, D. Chwa, and S.-K. Hong, "An estimation and compensation of the friction in an inverted pendulum," in *Proc. SICE-ICASE Int. Joint Conf.*, Oct. 2006, pp. 779–783.

[8] L. Fang, W. Ji Chen, and S. Un Cheang, "Friction compensation for a double inverted pendulum," in *Proc. IEEE Int. Conf. Control Appl. (CCA)*, Sep. 2001, pp. 908–913.

[9] M. Gäfvert, J. Svensson, and K. J. Astrom, "Friction and friction compensation in the furuta pendulum," in *Proc. Eur. Control Conf. (ECC)*, Aug. 1999, pp. 3154–3159.

[10] Z. B. Hazem, M. J. Fotuhi, and Z. Bingül, "Comparison of friction estimation models for rotary triple inverted pendulum," *Int. J. Mech. Eng. Robot. Res.*, vol. 8, no. 1, pp. 74–78, 2018.

[11] P. Grof and Y. Yam, "Furuta pendulum—A tensor product model-based design approach case study," in *Proc. IEEE Int. Conf. Syst., Man, Cybern.*, Oct. 2015, pp. 2620–2625.

[12] B. Bona, M. Indri, and N. Smaldone, "Nonlinear friction estimation for digital control of direct-drive manipulators," in *Proc. Eur. Control Conf. (ECC)*, Sep. 2003, pp. 2685–2690.

[13] P. E. Dupont, "Friction modeling in dynamic robot simulation," in *Proc. IEEE Int. Conf. Robot. Autom.*, May 1990, pp. 1370–1376.

[14] P. E. Dupont, "The effect of friction on the forward dynamics problem," *Int. J. Robot. Res.*, vol. 12, no. 2, pp. 164–179, 1993.

[15] F. Al-Bender and W. Symens, "Characterization of frictional hysteresis in ball-bearing guideways," *Wear*, vol. 258, nos. 11–12, pp. 1630–1642, Jun. 2005.

[16] V. Lampaert, J. Swevers, and F. Al-Bender, "Experimental comparison of different friction models for accurate low-velocity tracking," in *Proc. 10th Mediterranean Conf. Control Automat. (MED)*, Jul. 2002, pp. 1–9.

[17] M. J. Fotuhi, Z. B. Hazem, and Z. Bingul, "Comparison of joint friction estimation models for laboratory 2 DOF double dual twin rotor aero-dynamical system," in *Proc. 44th Annu. Conf. IEEE Ind. Electron. Soc. (IECON)*, Oct. 2018, pp. 2231–2236.

[18] D. Guida, F. Nilvetti, and C. M. Pappalardo, "Dry friction influence on inverted pendulum control," in *Proc. 3rd Int. Conf. Appl. Math., Simulation, Modelling*, Athens, Greece, 2009, pp. 29–31.

[19] C. Hu and F. Wan, "Parameter identification of a model with Coulomb friction for a real inverted pendulum system," in *Proc. Chin. Control Decis. Conf.*, Jun. 2009, pp. 2869–2874.

[20] A. C. Bittencourt, E. Wernholt, S. Sander-Tavallaey, and T. Brogårdh, "An extended friction model to capture load and temperature effects in robot joints," in *Proc. IEEE/RSJ Int. Conf. Intell. Robots Syst.*, Oct. 2010, pp. 6161–6167.

[21] L. Ding, X. Li, Q. Li, and Y. Chao, "Nonlinear friction and dynamical identification for a robot manipulator with improved cuckoo search algorithm," *J. Robot.*, vol. 2018, pp. 1–10, Jan. 2018.

[22] M. J. Fotuhi, Z. B. Hazem, and Z. Bingul, "Adaptive joint friction estimation model for laboratory 2 DOF double dual twin rotor aerodynamic helicopter system," in *Proc. 6th Int. Conf. Control Eng. Inf. Technol. (CEIT)*, İstanbul, Turkey, Oct. 2018, pp. 25–27.

[23] H. Yu, T. Xie, S. Paszczynski, and B. M. Wilamowski, "Advantages of radial basis function networks for dynamic system design," *IEEE Trans. Ind. Electron.*, vol. 58, no. 12, pp. 5438–5450, Dec. 2011.

[24] R. Zemouri, D. Racoceanu, and N. Zerhouni, "Recurrent radial basis function network for time-series prediction," *Eng. Appl. Artif. Intell.*, vol. 16, nos. 5–6, pp. 453–463, Aug. 2003.

- [25] R. Gencay and M. Qi, "Pricing and hedging derivative securities with neural networks: Bayesian regularization, early stopping, and bagging," *IEEE Trans. Neural Netw.*, vol. 12, no. 4, pp. 726–734, Jul. 2001.
- [26] N. Ekekewe, R. Etienne-Cummings, and P. Kazanzides, "Incremental encoder based position and velocity measurements VLSI chip with serial peripheral interface," in *Proc. IEEE Int. Symp. Circuits Syst.*, May 2007, pp. 3558–3561.
- [27] R. Pal, "Comparison of the design of FIR and IIR filters for a given specification and removal of phase distortion from IIR filters," in *Proc. Int. Conf. Adv. Comput., Commun. Control (ICAC)*, Dec. 2017, pp. 1–3.
- [28] S. Saxena, R. Jais, and M. K. Hota, "Removal of powerline interference from ECG signal using FIR, IIR, DWT and NLMS adaptive filter," in *Proc. Int. Conf. Commun. Signal Process. (ICCSP)*, Apr. 2019, pp. 0012–0016.
- [29] Y. Bao, Z. Hu, and T. Xiong, "A PSO and pattern search based memetic algorithm for SVMs parameters optimization," *Neurocomputing*, vol. 117, pp. 98–106, Oct. 2013.



ZIED BEN HAZEM received the bachelor's degree in mechanical engineering from the Higher Institute of Technological Studies, Rades, Tunisia, in 2011, and the master's degree in automatic control, robotics and information processing from the National School of Engineer of Carthage, Carthage University, in 2013. He is currently pursuing the Ph.D. degree in mechatronics engineering with the School of Engineering, Kocaeli University, Kocaeli, Turkey. His research interest in the control of a triple link rotary inverted pendulum.



MOHAMMAD JAVAD FOTUHI (Student Member, IEEE) received the B.Sc. degree in computer hardware engineering from Meybod Azad University, Yazd, Iran, in 2007, and the M.Sc. degree in mechatronics engineering from Sistan and Baluchestan University, Zahedan, Iran, in 2011. He is currently pursuing the Ph.D. degree in mechatronics engineering with Kocaeli University, Kocaeli, Turkey. He dedicated his thesis to the series elastic actuator in robotics. His research interests include are control, robotics, and fuzzy systems.



ZAFER BINGÜL (Member, IEEE) received the B.A. degree from Istanbul Technical University, Istanbul, Turkey, in 1992, and the M.S. and Ph.D. degrees from Vanderbilt University, Nashville, TN, in 1996 and 2000, respectively, all in electrical engineering. From 1999 to 2000, he was a Research Associate with the Electrical Engineering Department, Tennessee State University, Nashville, where he was engaged in research and application of genetic algorithms for multiobjective optimization problems. He is currently a Professor of mechatronics engineering with the School of Engineering, Kocaeli University, Kocaeli, Turkey. His research interests are robotics and welding automation, optimization, evolutionary algorithms, and control.

...